Erschienen in: Physical Review B ; 95 (2017), 15. - 155428
http://dx.doi.org/10.1103/PhysRevB.95.155428

PHYSICAL REVIEW B **95**, 155428 (2017)

Local electronic properties of the graphene-protected giant Rashba-split $BiAg_2$ surface

Julia Tesch,[1] Elena Voloshina,[2,*] Milan Jubitz,[1] Yuriy Dedkov,[1,†] and Mikhail Fonin[1,‡]
[1]*Fachbereich Physik, Universität Konstanz, 78457 Konstanz, Germany*
[2]*Humboldt-Universität zu Berlin, Institut für Chemie, 10099 Berlin, Germany*
(Received 29 December 2016; revised manuscript received 18 February 2017; published 19 April 2017)

We report the preparation of an interface between graphene and a strong Rashba-split $BiAg_2$ surface alloy and an investigation of its structure as well as the electronic properties by means of scanning tunneling microscopy/spectroscopy and density functional theory calculations. Upon evaluation of the quasiparticle interference patterns, an unperturbed linear dispersion for the π band of n-doped graphene is observed. Our results also reveal the intact nature of the giant Rashba-split surface states of the $BiAg_2$ alloy, which demonstrate only a moderate downward energy shift due to the presence of graphene. This effect is explained in the framework of density functional theory by an inward relaxation of the Bi atoms at the interface and subsequent delocalization of the wave function of the surface states. Our findings demonstrate a realistic pathway to prepare a graphene-protected giant Rashba-split $BiAg_2$ for possible spintronic applications.

DOI: 10.1103/PhysRevB.95.155428

Graphene has attracted much attention due to its unique transport, electronic, and elastic properties [1–3]. Taking into account these characteristics, many practical applications of graphene have been proposed. The most promising are graphene-based touch screens, which will potentially replace indium-tin-oxide (ITO-) based screens in the future [4,5], batteries and supercapacitors [6–8], and composite materials [9,10]. Above that, a single atom thick graphene layer can effectively protect the underlying material against oxidation and/or corrosion [11,12]. This property is particularly exciting when graphene is deposited or formed on the surface of a ferromagnet or a material which exhibits strong spin-orbit interaction [13–19]. Here, interfacial contact between graphene and the respective material might lead to the appearance of different new phenomena in graphene and at the interface, such as induced magnetism in graphene [20–22], possible induced spin-orbit splitting of the graphene π states [23,24], conservation of spin-polarized electron emission from the underlying ferromagnetic material [13,15], etc.

Previously published works on the adsorption of graphene on the surfaces of heavy materials, such as Ir(111) and Au(111), demonstrate that such contacts only weakly modify the dispersion of the spin-orbit split surface states of the metal surface. Adsorption of graphene merely leads to a rigid shift of the respective surface states to smaller binding energies [16,25,26], which was explained by the stronger localization of the surface state wave function, leading to a corresponding energy shift. At the same time, the intercalation of Au in the graphene/Ni(111) interface leads to the appearance of induced spin-orbit splitting of the graphene π states (up to $\approx$100 meV) as a result of the hybridization of these states and valence band states of the underlying heavy metal [23,24]. Here, the energetically unfavorable model of diluted Au atoms underneath graphene on Ni(111) was proposed [23]. However, recent scanning tunneling microscopy/spectroscopy (STM/STS) experiments have not shown any hints of such a splitting [27], leaving the question of induced spin-orbit interaction in graphene still open. In order to resolve this controversy and to evaluate the role of the substrate, further experiments on graphene, which is adsorbed on materials demonstrating a strong spin-orbit interaction, are required.

Here, we report the fabrication of protective graphene layers on a $BiAg_2$ surface alloy, which exhibits strongly Rashba-split surface states [28–30]. In this system, diluted Bi atoms form a $(\sqrt{3}\times\sqrt{3})R30^\circ$ structure. STM and STS used in the experiment allow one to carefully separate the quasiparticle interference (QPI) signatures arising from $BiAg_2$ and from graphene that gives a possibility to map the electronic structure of the graphene/$BiAg_2$ system around the Fermi level (E_F) in great detail. Our results show that the adsorption of graphene on the surface of an alloy only leads to a downward energy shift of the surface state without modifying its spin texture. We found that the π band of the n-doped graphene layer has a linear dispersion in the vicinity of the Dirac point (E_D) with $E_D = -400 \pm 30$ meV. Contrary to the results obtained in Ref. [23], our experimental and theoretical observations for graphene adsorbed on $BiAg_2$ rule out a considerable spin-orbit splitting of the graphene-derived π states around the K point ($<$18 meV). All experiments are systematically analyzed within the framework of the density functional theory (DFT) approach for the realistic experimental geometry, allowing one to acquire a profound understanding of the observed phenomena and discuss the possible use of this interface in future graphene-based spintronic applications. For details of the sample preparation, STM/STS experiments, and DFT calculations, see the Supplemental Material [31].

The sequence of preparation steps during the synthesis of the gr/$BiAg_2$ system (gr = graphene) is shown in Fig. 1 (see also Fig. S1 of the Supplemental Material for large scale STM images). In the first step, graphene nanoflakes (GNFs) of different sizes are prepared by means of a temperature programed growth (TPG) procedure from C_2H_4 on Ir(111), as described elsewhere [25,32]. A subsequent deposition of $\approx$70 Å of Ag on GNF/Ir(111) and annealing of this system at 450° C for 30 min leads to the formation of a GNF/Ag(111)/Ir(111) system with graphene flakes floating on top. Earlier experimental results [26] and the present STM/STS data confirm the high

*elena.voloshina@hu-berlin.de
†yuriy.dedkov@uni-konstanz.de
‡mikhail.fonin@uni-konstanz.de

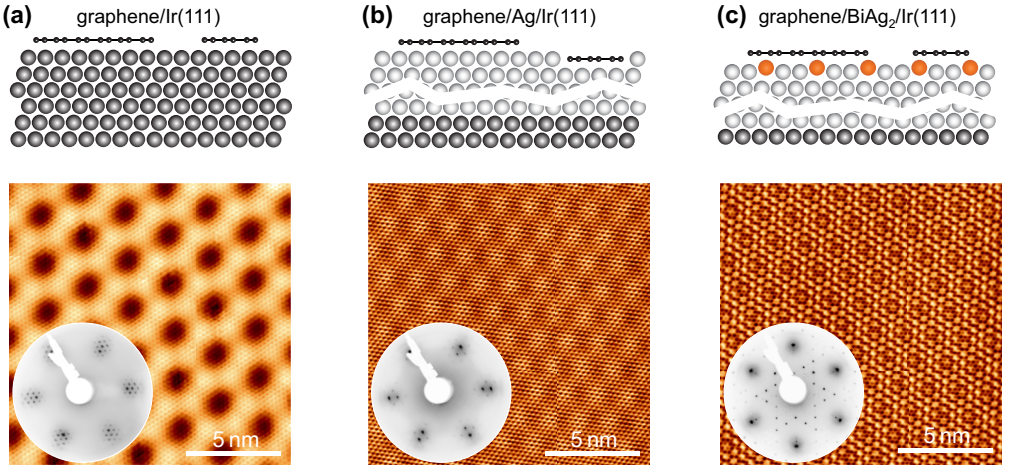

FIG. 1. (a) GNF/Ir(111), (b) GNF/Ag(111)/ Ir(111), and (c) GNF/$BiAg_2$/Ir(111). The bottom row shows the corresponding STM and LEED images acquired after every preparation step. Imaging parameters: (a) $U_T = 50$ mV, $I_T = 500$ pA; (b) $U_T = -150$ mV, $I_T = 800$ pA; (c) $U_T = 50$ mV, $I_T = 700$ pA. LEED images were obtained at 75 eV.

quality of such a system. In the next step, an almost stoichiometric $BiAg_2$ alloy is prepared underneath the GNFs via the adsorption of Bi atoms on GNF/Ag/Ir(111) at 200 °C and subsequent annealing at the same temperature for 30 min. This procedure leads to an effective intercalation of Bi atoms underneath the graphene layer, thus a $BiAg_2$ alloy with a $(\sqrt{3}\times\sqrt{3})R30^\circ$ structure with respect to Ag(111) is formed. The high quality of the formed GNF/$BiAg_2$ is confirmed by large scale STM and low-energy electron diffraction (LEED) experiments, where in the latter images one can clearly resolve diffraction spots from the graphene and $BiAg_2$ subsystems as well as the respective interference formed by these two sublattices. Incomplete coverage of the graphene layer in our prepared systems [see also Fig. 3(a)] allows one to carefully trace all changes in the electronic structure of the underlying metallic layer before and after graphene adsorption, as well as the corresponding modifications of the electronic properties of graphene with respect to those of a free-standing graphene layer.

In order to study the electronic band structure of the GNF/$BiAg_2$ system, we performed combined STM/STS experiments (Figs. 2 and 3). A large scale atomically resolved STM image and the respective dI/dV map of gr/$BiAg_2$ are presented in Figs. 2(a) and 2(b). Graphene forms a so-called moiré structure on the surface of the $BiAg_2$ alloy (see also Fig. 1), which has a (7×7) periodicity with respect to the graphene unit cell that corresponds to the (6×6) periodicity of the Ag(111) layer where Bi atoms form a $(\sqrt{3}\times\sqrt{3})R30^\circ$ structure [Fig. 4(a)]. A fast Fourier transform (FFT) of the dI/dV map yields the image presented in Fig. 2(c), where several characteristic features can be identified. The first one, which is marked by the dashed line hexagon, is assigned to the reciprocal lattice of a graphene layer [reciprocal vector $\vec{b}_{\rm gr}$ in Fig. 2(c)]. Each central spot here is surrounded by six additional ones, which are due to the moiré lattice formed at the gr/$BiAg_2$ interface. Bi atoms, which form a $(\sqrt{3}\times\sqrt{3})R30^\circ$ overstructure of the $BiAg_2$ alloy, are responsible for the respective spots in the FFT map [reciprocal vector $\vec{b}_{\rm Bi}$ in

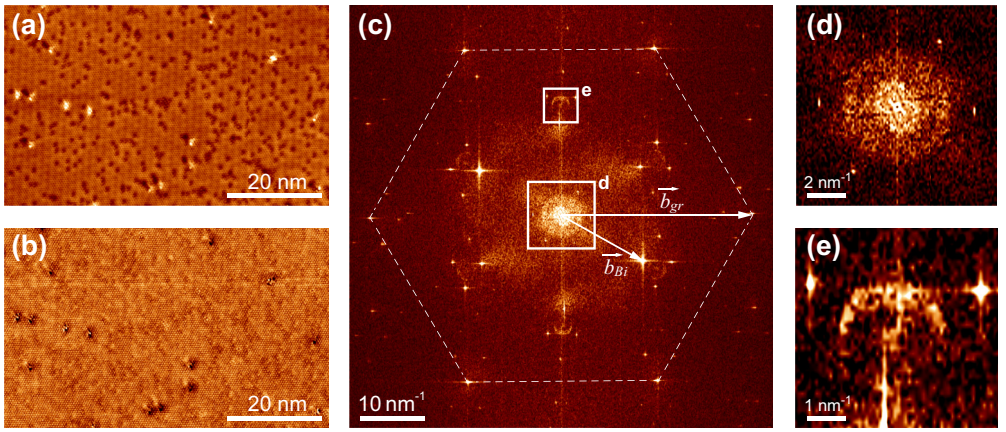

FIG. 2. (a) Topographic, $z(x,y)$, and (b) differential conductance, $dI/dV(x,y)$, maps acquired on GNF/$BiAg_2$. Imaging parameters: $U_T = +125$ mV, $I_T = 900$ pA, $f_{\rm mod} = 687$ Hz, $U_{\rm mod} = 10$ mV. (c) FFT image obtained from (b). The dashed hexagon marks the reciprocal lattice of graphene with vector $\vec{b}_{\rm gr}$. Vector $\vec{b}_{\rm Bi}$ marks the reciprocal lattice of $BiAg_2$. Rectangles are used for areas around the Γ point and the K point of the graphene BZ, zooms of which are shown in (d) and (e), respectively.

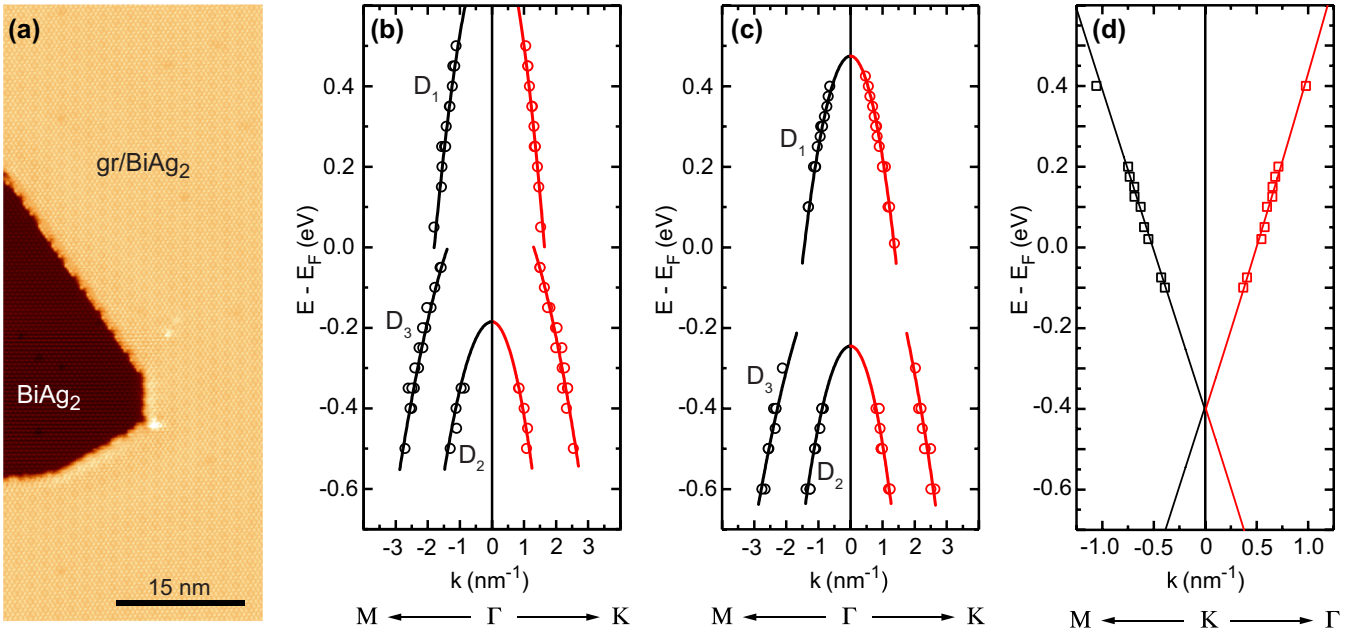

FIG. 3. (a) STM topography for the simultaneous imaging of areas of $BiAg_2$ and gr/$BiAg_2$. Imaging parameters: 75×30 nm^2, $U_T = 20$ mV, $I_T = 2$ nA. Scattering vector dispersions $k(E)$ obtained at different U_T corresponding to D_1, D_2, D_3 for (b) clean $BiAg_2$ and (c) gr/$BiAg_2$. (d) Scattering vector dispersion corresponding to the intervalley scattering in graphene for gr/$BiAg_2$.

Fig. 2(c)]. Analogously to the previous discussion, the six additional spots are resolved as well.

The most interesting features in the FFT can be identified around $\vec{q} = 0$ as well as around the $(\sqrt{3}\times\sqrt{3})R30^\circ$ points with respect to the graphene atomic lattice. The corresponding areas are marked by solid line rectangles, and their zooms are shown in Figs. 2(d) and 2(e), respectively. The discussed features in the FFT maps obtained from the dI/dV images acquired at different bias voltages (U_T) can be assigned to QPI

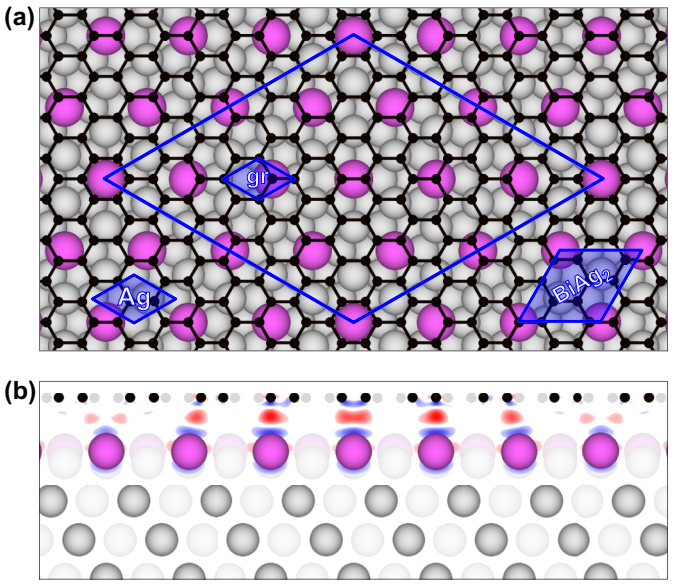

FIG. 4. (a) Top and (b) side views of the gr/$BiAg_2$ interface. In (b), the charge difference, $\Delta\rho_{gr/sub}(r) = \rho_{gr/sub}(r) - [\rho_{gr}(r) + \rho_{sub}(r)]$, is color coded, from red ($+2e$/nm^3) to blue ($-2e$/nm^3).

patterns formed after scattering of the electron waves at the surface defects (steps, dislocations, adatoms, vacancies, etc.). An analysis of such maps allows one to identify particular scattering vectors (q_E) between different electronic states in the Brillouin zone (BZ) at a fixed energy, $E = eU_T$, and to plot the energy dispersion of the carriers $E(k)$ around E_F.

The feature around $\vec{q} = 0$ shown in Fig. 2(d) is formed by the scattering vectors connecting different Rashba-split surface states of $BiAg_2$ and is very similar to the one observed earlier [29,30] (see Fig. S2 of the Supplemental Material for a series of FFT maps around $\vec{q} = 0$ obtained for gr/$BiAg_2$ at different U_T). Analysis performed in Refs. [29,30] allows one to identify them as D_1, D_2, and D_3 (the notation is according to Ref. [29]). They are marked by the respective symbols in Fig. S3 of the Supplemental Material, where the DFT calculated band structure of the $BiAg_2$/Ag(111) slab is shown. The zoom of the FFT presented in Fig. 2(e) reveals a "ringlike" structure. It is assigned to the intervalley scattering between graphene-related valence band states around the K and K' points. The radius of these rings is $2k$, where k is the wave vector of the Dirac particles at an energy E relative to E_F and it is measured with respect to the K point of the graphene BZ. The deviation of the shape of these ringlike features from the circle for large positive bias voltages is due to the trigonal warping at the energies far away from E_D, as was shown in theoretical calculations [33].

Figure 3 shows the extracted dispersions of the wave vector k gathered from a series of dI/dV maps measured for $BiAg_2$ and GNF/$BiAg_2$, as discussed above [see the STM image of the border between two regions in Fig. 3(a)]: Figs. 3(b) and 3(c) are for the Rashba-split surface states of $BiAg_2$ around the Γ point without and with a graphene layer on top, respectively, and Fig. 3(d) is for the graphene π states around the K point of the graphene-derived BZ. Analysis of the graphene dispersion

relation shows that graphene on $BiAg_2$ is n doped with a position of the Dirac point of $E_D = -400 \pm 30$ meV and a Fermi velocity of $(1.17 \pm 0.06) \times 10^6$ m/s, which is in good agreement with a value for nearly free-standing graphene on a metallic substrate [34,35].

A peculiar behavior is encountered upon comparison of Figs. 3(b) and 3(c), where the dispersions of the scattering vector for the surface state of $BiAg_2$ and GNF/$BiAg_2$ are presented, respectively. These data were obtained on the same sample under similar experimental conditions excluding any experimental or/and tip artifacts influencing the final result. One can clearly see that after adsorption of graphene on $BiAg_2$, all Rashba-split surface states are shifted downwards in energy by about 100–150 meV. A similar shift is detected for the single dI/dV spectrum measured as a function of U_T for the neighboring areas of $BiAg_2$ and gr/$BiAg_2$ (see Fig. S4 of the Supplemental Material). This effect is contrary to the previously observed results for graphene adsorption on Au(111) [25,26], Ag(111) [26,36,37], Cu(111) [38], and Ir(111) [16,39], where an upward energy shift for the metallic surface states was reported and explained by a stronger localization of the wave function of the metallic surface state producing an increase of Pauli repulsion at the interface. This effect leads to an increase of the energy of the electrons and consequently to the upward energy shift of the surface state. Moreover, recent angle-resolved photoemission spectroscopy (ARPES) experiments also reveal that adsorption of the atoms or molecules with closed shells such as rare gas Xe, C_{60}, iron octaethylporphyrin (FeOEP), or perylenetetracarboxylic dianhydride (PTCDA) on the surface of the $BiAg_2$ alloy does not lead to the energy shift of these Rashba-split states and k splitting remains intact [40,41].

In order to fully understand all observed effects we performed modeling of the electronic properties of the gr/$BiAg_2$ system in the framework of the DFT approach. For the modeling of the surface of the $BiAg_2$ alloy, $\frac{1}{3}$ of Ag atoms in the top layer of the seven-layer Ag(111) slab were replaced with Bi atoms, forming the characteristic $(\sqrt{3}\times\sqrt{3})R30^\circ$ superstructure. A graphene layer with a (7×7) periodicity was adsorbed on one side of this slab, which has a (6×6) periodicity with respect to the Ag(111) in-plane lattice. The resulting structure is shown in Figs. 4(a) and 4(b), where the formed moiré with a periodicity of 17.523 Å is clearly visible. The following systems were analyzed: (A) clean $BiAg_2$ surface after relaxation of the coordinates of the top Bi and Ag layers, (B) gr/$BiAg_2$ fixed, where the coordinates of the carbon atoms were fully relaxed and coordinates of the top layer of Bi and Ag atoms were fixed, as obtained for system A, and (C) gr/$BiAg_2$ relaxed, where the coordinates of the carbon atoms and the top layer of the Bi and Ag atoms were fully relaxed (see Table T1 of the Supplemental Material for the resulting interlayer distances for all considered structures). In our analysis of the electronic properties of the studied systems, the resulting band structures were unfolded on the (1×1) Brillouin zone of the respective sublattice, Ag(111) or graphene.

Figure 5 shows the unfolded band structures around the $\Gamma_{10}^{BiAg_2}$ point of BZ corresponding to the $BiAg_2$(111) unit cell for (a) $BiAg_2$ (system A), (b) gr/$BiAg_2$ fixed (system B), and (c) gr/$BiAg_2$ relaxed (system C). The choice of the $\Gamma_{10}^{BiAg_2}$ point [which coincides with the K_{00}^{Ag} point of the BZ corresponding to the Ag(111) unit cell] is caused by the appearance of an artificial Ag(111) surface state at $E - E_F = -100$ meV originating from the back side of the slab used in the DFT computation (see Figs. S5–S9 of the Supplemental Material for the additional figures). In Fig. 5(d) the band structure of graphene around the K_{00}^{gr} point of the graphene-derived BZ for the gr/$BiAg_2$ relaxed (system C) is shown.

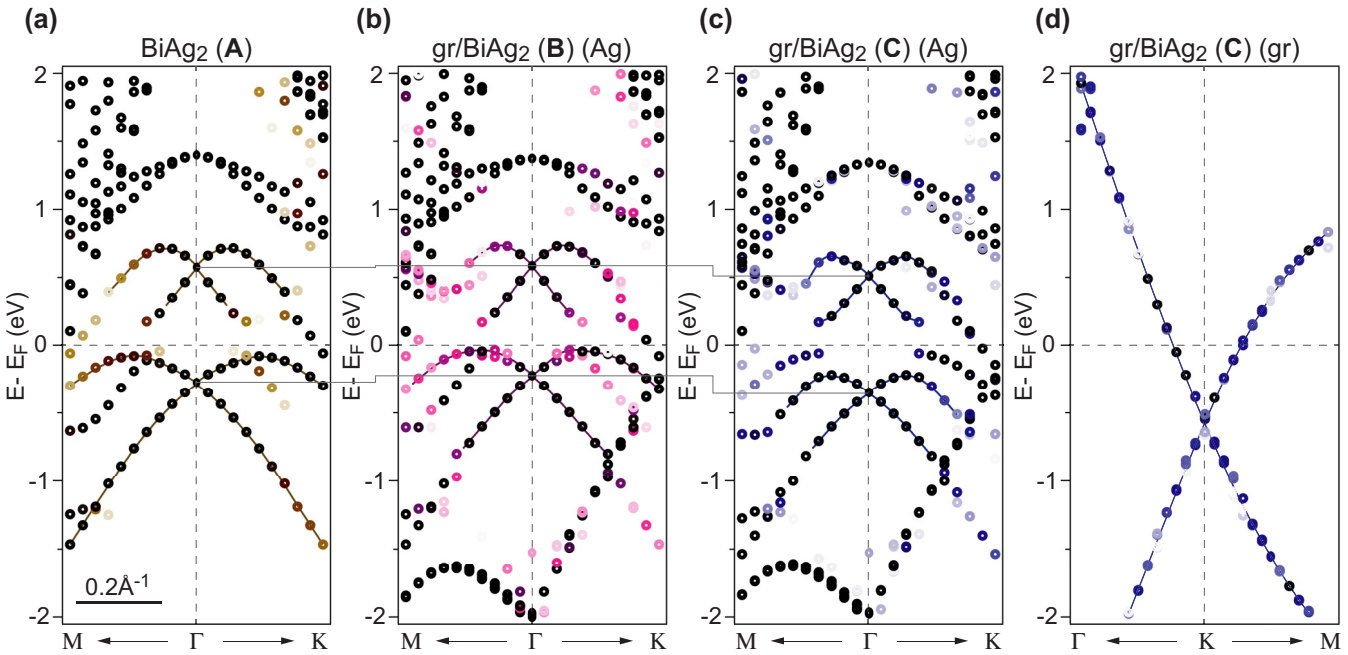

FIG. 5. Calculated energy band dispersions for (a) clean $BiAg_2$ (system A), (b) gr/$BiAg_2$ fixed (system B), and (c), (d) gr/$BiAg_2$ relaxed (system C).

The DFT calculations performed for the above described systems confirm our experimental observations for the downward energy shift of the $BiAg_2$ surface state after graphene adsorption. In Fig. 5(a) the dispersions of the Rashba-split surface states for a clean $BiAg_2$ surface are clearly resolved. The energy positions of the crossing points of the Rashba-split surface states at the $\Gamma_{10}^{BiAg_2}$ point are -280, 575, and 1395 meV, respectively. Adsorption of graphene on the surface of the alloy, without relaxation of the atomic positions for the Bi and Ag top layers, leads to an upward energy shift of all states and the resulting energy positions of the crossing points are -225, 585, and 1395 meV, respectively [Fig. 5(b)]. This effect can be explained by a stronger localization of the surface state wave functions that leads to an increase of Pauli repulsion for these states and thus to the energy shift to smaller binding energies.

The relaxation of all atomic positions at the interface between graphene and the $BiAg_2$ alloy, which models the real experimental situation, leads to the opposite effect compared to the previously described case [Fig. 5(c)]. Here, we observed a relatively large downward energy shift of the Rashba-split surface states of $BiAg_2$. The energy positions of the crossing points at the $\Gamma_{10}^{BiAg_2}$ point are -355, 515, and 1340 meV, respectively. Our calculations show that the adsorption of graphene on the surface of a $BiAg_2$ alloy leads to an inward Bi-atom relaxation with a reduction of the mean distance between planes formed by Bi and Ag atoms by 0.12 Å. At the same time, the mean distance between graphene and the top Bi layer is slightly increased from 3.219 Å for $BiAg_2$ fixed (system B) to 3.277 Å for $BiAg_2$ relaxed (system C). Both effects lead to a stronger delocalization of the wave function of the surface states compared to the clean surface of the $BiAg_2$ alloy. Thus the reduction of Pauli repulsion in turn leads to an increase of the binding energies of all surface states upon graphene adsorption. The effect of delocalization can be visualised via a two-dimensional (2D) presentation (side and top view) of the calculated electron localization function (ELF) [42–45]. The analysis of ELF presented in Fig. S10 of the Supplemental Material confirms the effect of stronger delocalization of the surface state for the gr/$BiAg_2$-relaxed system (system C), compared to the previous case of a non-fully-relaxed system (system B).

Our DFT results show that graphene is n doped in both cases of its adsorption on $BiAg_2$ (fixed or relaxed structure) with a position of the Dirac point of $E_D - E_F = -545$ meV (system B) and $E_D - E_F = -590$ meV (system C) [Fig. 5(d)]. This value is in reasonably good agreement with the doping level of graphene of -400 ± 30 meV obtained in the STM/STS experiments. Our calculations demonstrate the absence of an energy gap at E_D for gr/$BiAg_2$ fixed and the opening of the gap for the graphene π states of $\approx$95 meV at E_D for the gr/$BiAg_2$-relaxed system. Despite the presence of a substrate underneath graphene, which demonstrates a strong spin-orbit interaction, no spin splitting for the graphene-derived π states is found in experiments as well as in the DFT calculations. This can be explained by the relatively large gr-Bi distance of $\approx$3.3 Å in the studied systems. These results are also confirmed by our STM/STS experiments where no evidence of the splitting of the graphene states leading to modifications of the relevant scattering features was observed. However, we believe that further studies by means of ARPES (spin-ARPES) might shed more light on the possible existence of an energy gap in the graphene band structure as well as on the spin texture of the valence band states in the vicinity of E_F for the gr/$BiAg_2$ system.

In summary, we demonstrated the successful preparation of graphene on a strong Rashba-split $BiAg_2$ surface alloy via subsequent intercalation of Ag and Bi in graphene/Ir(111). Our method grants large flexibility in the fabrication of big and small graphene flakes in this system. The systematic STM/STS experiments presented show that graphene on $BiAg_2$ is n doped with a position of the Dirac point of -400 ± 30 meV below E_F and that the π states have a linear dispersion, confirming the massless nature of carriers in the vicinity of the Fermi level. In contrast to the previously studied cases of a graphene adsorption on noble metal surfaces, here we observed a downward shift of the giant Rashba-split surface states of the $BiAg_2$ surface alloy for a graphene covered surface compared to a clean one, rendering the spin texture of the graphene-protected $BiAg_2$ surface alloy unaffected by graphene adsorption. Our experimental findings were analyzed in the framework of the DFT approach, where an inward relaxation of the Bi atoms in $BiAg_2$ upon graphene adsorption was found, consequently leading to the delocalization of the surface state wave function. Despite the presence of a strong Rashba-split $BiAg_2$ surface alloy in contact with graphene, no sizable spin splitting (above 18 meV) was detected for the graphene π states, as confirmed by our STM/STS and DFT results. The studied system, where a lattice of diluted Bi atoms is placed underneath graphene on Ag(111), is a perfect model example demonstrating a strong Rashba splitting of the surface states and the absence of induced spin-orbit splitting in graphene. The results presented solve the controversy on the possible observation of spin-splitting phenomena in graphene physisorbed on metallic surfaces with large Rashba splitting.

We thank the German Research Foundation (DFG) for financial support within the Priority Programme 1459 "Graphene" and the North-German Supercomputing Alliance (HLRN) for providing computer time.

[1] A. K. Geim and K. S. Novoselov, Nat. Mater. **6**, 183 (2007).
[2] A. Castro Neto, F. Guinea, N. Peres, K. Novoselov, and A. Geim, Rev. Mod. Phys. **81**, 109 (2009).
[3] A. Geim, Science **324**, 1530 (2009).
[4] S. Bae, H. Kim, Y. Lee, X. Xu, J.-S. Park, Y. Zheng, J. Balakrishnan, T. Lei, H. R. Kim, Y. I. Song *et al.*, Nat. Nanotechnol. **5**, 574 (2010).
[5] J. Ryu, Y. Kim, D. Won, N. Kim, J. S. Park, E.-K. Lee, D. Cho, S.-P. Cho, S. J. Kim, G. H. Ryu *et al.*, ACS Nano **8**, 950 (2014).
[6] G. Wang, B. Wang, X. Wang, J. Park, S. Dou, H. Ahn, and K. Kim, J. Mater. Chem. **19**, 8378 (2009).
[7] H. Kim, K.-Y. Park, J. Hong, and K. Kang, Sci. Rep. **4**, 5278 (2014).

[8] M. F. El-Kady, Y. Shao, and R. B. Kaner, Nat. Rev. Mater. **1**, 16033 (2016).
[9] S. Stankovich, D. Dikin, G. Dommett, K. Kohlhaas, E. Zimney, E. Stach, R. Piner, S. Nguyen, and R. Ruoff, Nature (London) **442**, 282 (2006).
[10] X. Huang, X. Qi, F. Boey, and H. Zhang, Chem. Soc. Rev. **41**, 666 (2012).
[11] E. Sutter, P. Albrecht, F. E. Camino, and P. Sutter, Carbon **48**, 4414 (2010).
[12] M. J. Nine, M. A. Cole, D. N. H. Tran, and D. Losic, J. Mater. Chem. A **3**, 12580 (2015).
[13] Y. S. Dedkov, M. Fonin, and C. Laubschat, Appl. Phys. Lett. **92**, 052506 (2008).
[14] Y. S. Dedkov, M. Fonin, U. Ruediger, and C. Laubschat, Appl. Phys. Lett. **93**, 022509 (2008).
[15] B. Dlubak, M.-B. Martin, R. S. Weatherup, H. Yang, C. Deranlot, R. Blume, R. Schloegl, A. Fert, A. Anane, S. Hofmann *et al.*, ACS Nano **6**, 10930 (2012).
[16] A. Varykhalov, D. Marchenko, M. R. Scholz, E. D. L. Rienks, T. K. Kim, G. Bihlmayer, J. Sanchez-Barriga, and O. Rader, Phys. Rev. Lett. **108**, 066804 (2012).
[17] A. Varykhalov, J. Sánchez-Barriga, D. Marchenko, P. Hlawenka, P. S. Mandal, and O. Rader, Nat. Commun. **6**, 7610 (2015).
[18] Z. Wang, D.-K. Ki, H. Chen, H. Berger, A. H. MacDonald, and A. F. Morpurgo, Nat. Commun. **6**, 8339 (2015).
[19] E. C. T. O'Farrell, J. Y. Tan, Y. Yeo, G. K. W. Koon, B. Özyilmaz, K. Watanabe, and T. Taniguchi, Phys. Rev. Lett. **117**, 076603 (2016).
[20] M. Weser, Y. Rehder, K. Horn, M. Sicot, M. Fonin, A. B. Preobrajenski, E. N. Voloshina, E. Goering, and Y. S. Dedkov, Appl. Phys. Lett. **96**, 012504 (2010).
[21] M. Weser, E. N. Voloshina, K. Horn, and Y. S. Dedkov, Phys. Chem. Chem. Phys. **13**, 7534 (2011).
[22] D. Usachov, A. Fedorov, M. M. Otrokov, A. Chikina, O. Vilkov, A. Petukhov, A. G. Rybkin, Y. M. Koroteev, E. V. Chulkov, V. K. Adamchuk *et al.*, Nano Lett. **15**, 2396 (2015).
[23] D. Marchenko, A. Varykhalov, M. R. Scholz, G. Bihlmayer, E. I. Rashba, A. Rybkin, A. M. Shikin, and O. Rader, Nat. Commun. **3**, 1232 (2012).
[24] A. M. Shikin, A. G. Rybkin, D. Marchenko, A. A. Rybkina, M. R. Scholz, O. Rader, and A. Varykhalov, New J. Phys. **15**, 013016 (2013).
[25] P. Leicht, L. Zielke, S. Bouvron, R. Moroni, E. Voloshina, L. Hammerschmidt, Y. S. Dedkov, and M. Fonin, ACS Nano **8**, 3735 (2014).
[26] J. Tesch, P. Leicht, F. Blumenschein, L. Gragnaniello, M. Fonin, L. E. M. Steinkasserer, B. Paulus, E. Voloshina, and Y. Dedkov, Sci. Rep. **6**, 23439 (2016).
[27] P. Leicht, J. Tesch, S. Bouvron, F. Blumenschein, P. Erler, L. Gragnaniello, and M. Fonin, Phys. Rev. B **90**, 241406 (2014).
[28] C. R. Ast, J. Henk, A. Ernst, L. Moreschini, M. C. Falub, D. Pacilé, P. Bruno, K. Kern, and M. Grioni, Phys. Rev. Lett. **98**, 186807 (2007).
[29] L. El-Kareh, P. Sessi, T. Bathon, and M. Bode, Phys. Rev. Lett. **110**, 176803 (2013).
[30] S. Schirone, E. E. Krasovskii, G. Bihlmayer, R. Piquerel, P. Gambardella, and A. Mugarza, Phys. Rev. Lett. **114**, 166801 (2015).
[31] See Supplemental Material at http://link.aps.org/supplemental/10.1103/PhysRevB.95.155428 for experimental and computational details; Additional STM/STS and DFT results.
[32] J. Coraux, A. T. N'Diaye, M. Engler, C. Busse, D. Wall, N. Buckanie, F.-J. M. zu Heringdorf, R. van Gastel, B. Poelsema, and T. Michely, New J. Phys. **11**, 023006 (2009).
[33] L. Simon, C. Bena, F. Vonau, M. Cranney, and D. Aubel, J. Phys. D: Appl. Phys. **44**, 023006 (2011).
[34] P. E. Trevisanutto, C. Giorgetti, L. Reining, M. Ladisa, and V. Olevano, Phys. Rev. Lett. **101**, 226405 (2008).
[35] C. Hwang, D. A. Siegel, S.-K. Mo, W. Regan, A. Ismach, Y. Zhang, A. Zettl, and A. Lanzara, Sci. Rep. **2**, 590 (2012).
[36] W. Jolie, F. Craes, and C. Busse, Phys. Rev. B **91**, 115419 (2015).
[37] M. Garnica, M. Schwarz, J. Ducke, Y. He, F. Bischoff, J. V. Barth, W. Auwärter, and D. Stradi, Phys. Rev. B **94**, 155431 (2016).
[38] H. González-Herrero, P. Pou, J. Lobo-Checa, D. Fernández-Torre, F. Craes, A. J. Martinez-Galera, M. M. Ugeda, M. Corso, J. E. Ortega, J. M. Gomez-Rodriguez *et al.*, ACS Nano **10**, 5131 (2016).
[39] D. Subramaniam, F. Libisch, Y. Li, C. Pauly, V. Geringer, R. Reiter, T. Mashoff, M. Liebmann, J. Burgdörfer, C. Busse *et al.*, Phys. Rev. Lett. **108**, 046801 (2012).
[40] L. Moreschini, A. Bendounan, C. R. Ast, F. Reinert, M. Falub, and M. Grioni, Phys. Rev. B **77**, 115407 (2008).
[41] M. C. Cottin, J. Lobo-Checa, J. Schaffert, C. A. Bobisch, R. Möller, J. E. Ortega, and A. L. Walter, New J. Phys. **16**, 045002 (2014).
[42] A. D. Becke and K. E. Edgecombe, J. Chem. Phys. **92**, 5397 (1990).
[43] A. Savin, R. Nesper, S. Wengert, and T. F. Fassler, Angew. Chem., Int. Ed. **36**, 1809 (1997).
[44] L. De Santis and R. Resta, Surf. Sci. **450**, 126 (2000).
[45] Y. Qi, L. G. Hector, Jr., N. Ooi, and J. B. Adams, Surf. Sci. **581**, 155 (2005).